Indian Journal of Geo Marine Sciences
Vol. 49 (10), October 2020, pp. 1619-1626

Efficient pre-processing and retrieval of reflectance using calibration modules for Hyperspectral satellite data (Hyperion) and denoising of Hyperspectral reference spectra using wavelet based Adaptive Bilateral Filtering (HABF) -A case study on mangroves forest in Muthupet lagoon, Tamil Nadu

A Selvaraj[†] & S Saravanan*[,$]

Department of Civil Engineering, National Institute of Technology, Tiruchirappalli, Tamil Nadu – 620 015, India

[E-mail: [†]selvaphdnit@gmail.com; [$]ssaravanan@nitt.edu]

Received 12 January 2019; revised 09 December 2019

The article invoves in the preprocessing of hyperion data, and denoising of hyperspectral reference spectral library, which is generated from the spectro-radiometer. The atmospheric correction module like Fast Line-of-sight of Atmospheric Analysis of Spectral Hypercubes provided the smooth absolute spectral profile. In connection to that, the Hybrid Adaptive Bilateral Filter (HABF) is proposed for denoising of field based spectral library, and laboratory based spectral library. To implement the proposed algorithm, spectral library of mangrove has been exploited, which is collected from Muthupet mangrove forest, and spectra of particular species is generated from Field-spectro-radiometer with wavelength ranges from 350 nm to 2500 nm, and 10 nm band width. This spectral library has been used as an input signal since it contains noise across wavelength ranges from 350 – 450 nm, 1000 – 1200 nm, and 2000 – 2500 nm due to atmospheric conditions. These noises can be removed effectively by the proposed wavelet based HABF techniques and conventional method of denoising. The performance of each method was compared with performance evaluation parameter such as PSNR and MSE

[**Keywords**: Bilateral filter, Destriping, Digital number to radiance, FLAASH, Hyperion data]

Introduction

The Hyperspectral remote sensing is defined as the simultaneous acquisition of images in many narrow contiguous spectral bands[1-4]. It focuses primarily on advanced land imaging techniques[5-6]. The wavelength regions ranges from 300 to 1000 nm having about 70 bands, and then operates in the Shortwave Infrared Region (SWIR) with a wavelength of 900 to 2500 nm having 172 bands[5]. The hyperspectral data provides three-dimensional data cube (Fig. 1).

The hyperspectral image is a huge data since it contains larger number of bands. Though it has numerous bands, not all bands are necessary to be incorporated into the analysis to attain qualitative and quantitative remote sensing data[7]. As Hyperion is also a push broom type sensor and generate error in the very near infrared (VNIR) and short wave infrared (SWIR) region, which is appeard as a vertical strip in the images[8-9]. These errors must be corrected before data processing and pre-processing the data is vital for enhancing the classification accuracy[10]. Atmospheric correction is broadly used in hyperspectral images to derive reflectance from the radiance image. Several commercial packages are available to carry out the atmospheric correction process, such as Atmospheric and Topographic Correction (ATCOR 4)[11], Atmospheric Correction (ACORN 4.1)[12], (FLAASH)[13] and High accuracy and Atmospheric accuracy

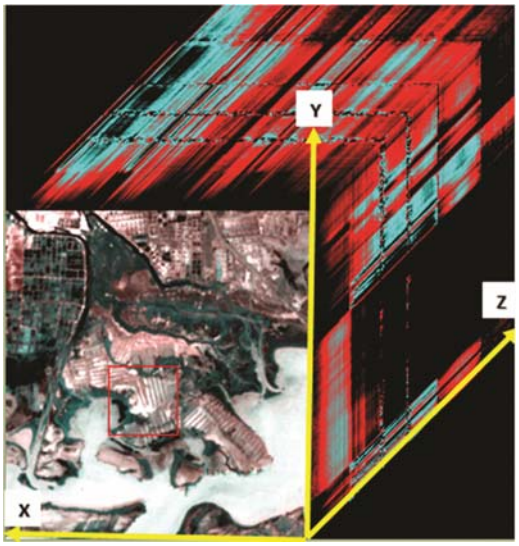

Fig. 1 — Hyperion image cube R-3D (752.43 nm), G-3D (650.67 nm), and B-3D (548.920 nm)

Correction for Hyperspectral data (HATCH)[14]. FLAASH and QUAC algorithms are widely used for atmospheric correction while FLAASH provides better results[15-17]. MODTRAN based FLAASH provides well-adjusted output from the atmospheric correction parameter, water vapour column and aerosol from the image[18-21]. Various researchers have carried out preprocessing of hyperspectral imagery in their research[22-27]. Denoising is one of the essential tasks in image processing that enhance the quality of information in the image[28]. Most of hyperspectral based imagery has been affected severely by existing noise. Therefore it is very much essential to preprocess the noisy spectra of hyper spectral sensor.

Remote sensing techniques have been widely used in past decades for the activities of mangrove ecosystems of India[29,30]. Due to inherent variations in the detector's sensitivity and the warm-up period required by the instrument, detectors response at VNIR (3.5 – 1.0 μm) and SWIR 2 regions (1.8 – 25 μm). Some portion of electromagnetic radiation taking journey through the atmosphere is absorbed by the water vapour present in the atmosphere, and hence, the reflectance from the particular target has been affected by adverse noise[31]. A new field-based Push broom Imaging Spectrometer (PIS) was developed by Zhang *et al*.[32] and the imaging spectro-radiometer coupled with more noise signal, which due to physical instruments, sun's illumination, field environment complex condition and others[33]. The Hyperspectral imaging system is the imaging techniques in one system to offer comprehensive information of object, which otherwise cannot be achieved with either conventional imaging or spectroscopy alone[34]. Many denoising techniques exist at literature, such as denoising the spectra based on Mexican hat wavelet[35], the wavelet based spectroscopy and spectral analysis[36], noise reduction of hyperspectral data using single spectral analysis proposed[37-39]. The proposed method provides excellent performance when compared to conventional median filter and center weighted threshold value for median (CWM) filter. Andria *et al*.[40] proposed a method that consists of liner filtering of only the vertical and diagonal details of the image, and the 1st level 2D wavelet decomposition is carried out for the image. Prasad *et al*.[41] used Moving average and Savitzky-Golay method to remove the self generated noise presented in the spectral profile obtained from hyperspectral sensor[42]. The central objective of the article is to perform preprocessing of the hyperspectral image efficiently for the selected study. This study emphasises the importance of each preprocessing procedure and the ways to overcome the shortfalls in the previously used preprocessing methods to obtain efficiently corrected data to achieve accurate results from the hyperspectral imagery. In addition, this article attempted the noise reduction of spectra of mangrove species, which obtained from field Spectro-radiometer. It is the first attempt to propose the wavelet based denoising techniques such as Hybrid wavelet adaptive bilateral filtering and performance of each techniques in terms of Peak Signal to Noise Ratio (PSNR), and MSE (Mean Square Error) evaluated.

Materials and Methods

Case study and image data used

In present study EO-1 Hyperion (EO1H1420532012272110KZ_PF2_01) data obtained from the www.earthexplorer.usgs.gov website dated on 29.09.2012 is exploited. This Hyperion image data set has to undergo preprocessing before further analysis. Level 1Gst is HDF format and was calibrated to obtain the radiance values provided as a 16-bit integer. The Muthupet mangroves forest is located at the southernmost end of the Cauvery delta, Tiruvarur District, Tamil Nadu, India which lies between 10°22'33'' N and 79°29'33'' E (Fig. 2). In the study area, six mangrove species are available in which the *Avicennia marina* is dominant and its breadth varies from a few meters to 2.5 km. The Muthupet mangroves receive freshwater mostly through the northeast monsoon season from October to November[29]. The drained rivers in the study area are Paminiyar, Koraiyar, Kilaithankiyar, Marakkakoraiyar, and other tributaries of the river Cauvery flow through Muthupet and adjacent village. For study purpose, the Hyperion image is cropped spatially by 217×235 pixel size which covers mangrove, sand-dunes, saltpan, agriculture and barren land. To run proposed algorithm, sample of mangrove

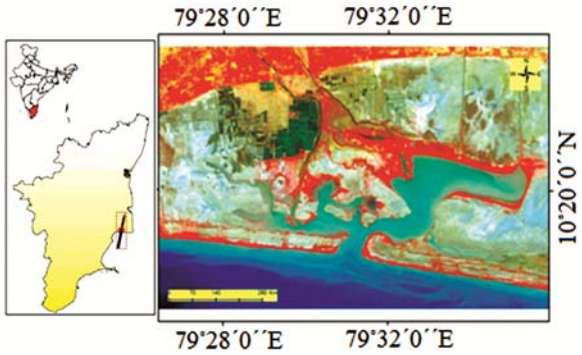

Fig. 2 — Location of the study area

Table 1 — Specification of the used hyperspectral image

Data set attribute	Attribute values
Spectral range	0.4-2.5 μm
Spatial resolution	30 m
Spectral resolution	10 nm
Radiometric resolution	16 bits/pixel
Swath Width	7.5 km
Acquisition data	2012/09/28
Cloud cover	10 % to 19 %
Orbit path	141
Orbit row	53
Processing Level	L1Gst
Sun Azimuth	110.630587
Sun Elevation	57.197791

species is picked from Muthupet mangrove forest, and spectra of particular species was obtained from ASD Spectro-radiometer. The specification of data that have used mentioned in Table 1.

Methodology

Band selection (Bad bands removal)

The primary step is the selection of bands to overcome the redundancy in the spectral bands of the hyperspectral image. By dropping the redundant data, one can shorten the processing times and improve the object recognition accuracy. The hyperion level 1G data has 242 bands of which only 198 are non-zero due to the low response of the detector. Thus out of 242 bands, only 198 bands requires calibration. The hyperion data is therefore processed with the calibrated 198 non-zero bands (bands 1 to 7 and 225 to 242 intentionally removed) for mangrove species matching). In this study, among the 198 non-zero bands, some of them fall in the overlap region of the two Spectro-radiometer, (bands 56 to 78) thus the bands 77 and 78 are ignored due to the presence of their higher noise level which leaves us with 196 unique bands. In addition to the water vapour absorption bands, the other bands which have to be eliminated and were identified to be bands 120 to 132 (1346 to 1467 nm), bands 165 to 182 (1800 to 1971 nm) and bands 221 (above 2356 nm) and higher. Water absorption band absorbs all the incident solar energy and are visually identified. Finally, 162 bands are chosen. The list of bands which are eliminated including the water absorption bands is given below in Table 2. The band selection can be carried out using the basic tool in ENVI 'Resize the data'. The Figure 3 shows the flowchart which involves both preprocessing and denoising techniques.

Table 2 — List of unused bands of the Hyperion sensor

Bands	Description
1 to 7	Not illuminated
58 to 78	Overlap region
120 to 132	Water absorption band
165 to 182	Water absorption band
185 to 187	Identified by bad band list
221 to 224	Water absorption band
225 to 242	Not illuminated

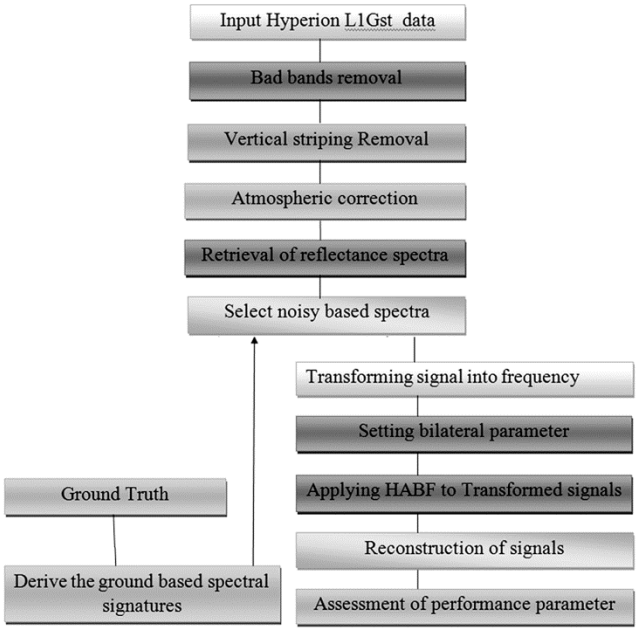

Fig. 3 — Flow chart for methodology

Bad column removal

In Hyperion datasets, due to the poor response from the detectors, the majority of the abnormal pixels in the image appear as vertical strips[5]. After visualization of each band, it is found that bad columns 108 and 182 which exist in bands 8, bad column 118-120 exist in band 9. These bad columns weeded out by taking the average of the adjacent pixels, either with a 4-pixel average (the average of the four nearest neighbours) or with an 8-pixel average (the average of the eight nearest neighbours). This can be performed using the pixel editor tool of the image window in ENVI module.

DN to radiometric calibration

The radiance is said to be the amount of radiation that comes from a target area. Since FLAASH module can accept the image only as radiance values, the conversion of the DN values to radiance values is mandatory. Two scaling factor is required for the

VNIR and SWIR bands. The Radiance L (W/m^2 /μm/ sr) is computed using the formula L = DN/40 for VNIR bands and L = DN/80 for SWIR bands.

FLAASH module

ENVI's FLAASH module is used for retrieving the spectral reflectance from the hyperspectral radiance images. It compensates the atmospheric effects and corrects the wavelengths in the visible region of the electromagnetic spectrum through NIR and SWIR region. FLAASH has inbuilt support for hyperspectral sensors.

Denoising using hybrid adaptive bilateral filtering using discrete wavelet transform

It mainly involves three stages, which are (i) Signal decomposition, (ii) Noise removal using proposed filter, and (iii) Performance assessment. The input signal is decomposed into low frequency component, and high frequency component using discrete wavelet transform. In this article, the sym4 wavelet has been used for decomposition of signal. After decomposition of signal, adaptive bilateral filter is applied to transformed component, it is a modified filter from bilateral filter. Riechert *et al*.[44] explored that the non local, and bilateral filter have a new adaptive version as follows.

$$BF^*[u]_x = \frac{1}{Wx}\sum_{y\in B\tau(x)} G\sigma r\,(||x-y||)G_{\sigma r}(||u(x)\text{-}u(y)||)\,u(y) \quad \ldots (1)$$

$$\text{Where, } W_x = \sum_{y\in B\tau(x)} G\sigma r\,(||x-y||)\,G_{\sigma r}(||u(x)\text{-}u(y)||) \quad \ldots (2)$$

Where, $B\tau(x)\ is$ set of neighbours of x that is similar to x.

The denoising steps of the noisy spectral profile using discrete wavelet transform based on HABF filtering techniques are described as follows: mangrove spectral profile takes up noisy signal generated from ASD, and it contains noise at the wavelength of 350-450 nm, 100-1200 nm, and 2000-2500 nm of spectral profile which is used as an input for denoising model. The input signal was then decomposed into low and high frequency component. The standard deviation is the crucial parameter that controls the output of spectral profile, the bilateral filter half-width, and bilateral filter standard deviation assigned as follows. The IDWT can be applied to both high level, and low level transformed signal using sym4 wavelet. The performance parameters such as MSE and PSNR can be evaluated in order to check the filtering performance on noisy signal. In signal processing, MSE or Minimum Squared Deviation (MSD) of an estimator, which estimates unobserved quantity, and measure the average of the square of the error. The ratio frequently used as a measurement in terms of quality between original and denoised signal. The denoising effect is proportional to PSNR and is inversely proportional to MSE, and are represented as follows:

$$\text{PSNR} = 10\log\frac{\sum_{i=1}^{n}(\rho_i)^2}{\sum_{i=1}^{n}(\hat{\rho}_i-\rho_i)^2} \quad \ldots (3)$$

$$\text{MSE} = n^{-1}\sum_{i=0}^{n}(\hat{\rho}-\rho)^2 \quad \ldots (4)$$

Finally, the output results of proposed system were compared with the existing algorithm such as Savithzky-Golay and Moving average method. Savitzky-Golay filter performed the middle position and neighbors in the spectrum. Tsai & Philpot[41] disussed the filter size an important parameter in moving average method, which takes the mean spectral value of all points within a particular window since new value of the focal point of the window. This method is exclusively based on linear computation.

Results and Discussion

Effect of bad column

In present work, we are addressing the bad column removal which is mandatory to improve the reflectance. After selecting a good number of bands, the bad columns can be found in the columns from 435 to 538 in band 8; similarly, in bands 9 and 10 bad columns are between 435-465 and 435-445, respectively. It is required to correct the bad column in the Hyperion images. This de-striping can be achieved by taking the average of adjacent columns in the corresponding band. The value of each bad pixel of the concerned column is shown as a negative value in the atmospherically corrected reflectance image. Figures 4(a, c and e) contains the bad columns. After the computation of the average of neighbourhood pixels (average of 4 pixel or average 8 pixels), the bad pixel is replaced with the new average value. As a result, it transforms into a destriped image which is shown in Figures 4(b, d and f).

Atmospheric correction results-FLAASH

Once essential bands have been selected based on the application of the FLAASH model, which run on few parameters such as the radiance data, sensor type, mean ground elevation, scene centre location and flight time and sensor altitude should be provided as input for processing the radiance data. In Figures 5(a and b), we

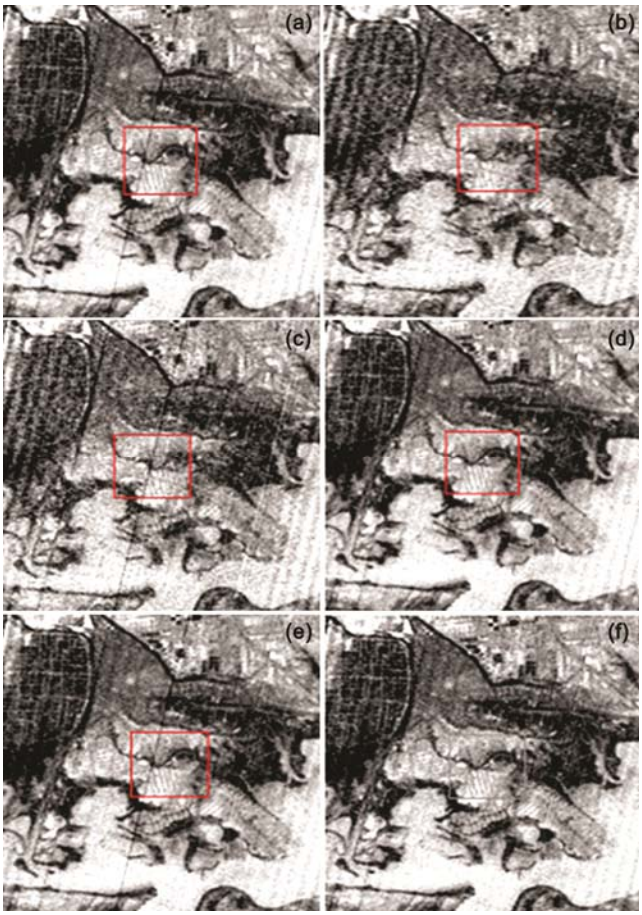

Fig. 4 — Bad column removal: (a) Bad column present at band 8, (b) After removing bad column of band 8, (c) Bad column present at band 9, (d) After removing bad column of band 9, (e) bad column present at band 10, and (f) after removing bad column of band 10

can discriminate visually. There exists an evident difference in the feature before and after preprocessing, i.e. by seeing the spectral signature in Figure 5(b), there exist variations in reflectance with respect to the wavelength. In this study, we primarily focus our attention on mangrove feature. In Figure 5(b), we can observe the invisible portion in the spectrum, the chlorophyll available in the vegetation absorbs the blue and red wavelength more extremely than green therefore generates a small reflectance peak within a green wavelength in the spectrum. The reflectance abruptly surges across the boundary between red and infrared wavelengths because of interaction with the internal cellular structure of leaves.

Conversion of negative value from reflectance image result

Sometimes FLAASH output may lead to negative DN pixels, to avoid this and to convert the reflectance values between 0 to 1, the equation 5 is used. If the

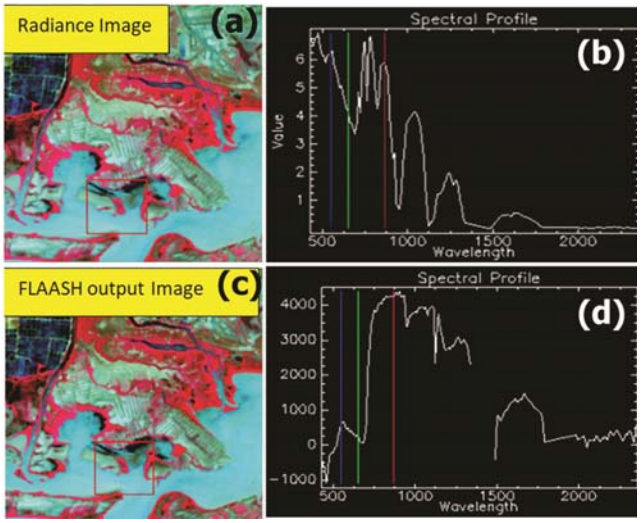

Fig. 5 — Atmospheric results: (a, b) Spectral curve of mangrove before atmospheric correction, and (c, d) Spectral curve of mangrove after atmospheric correction

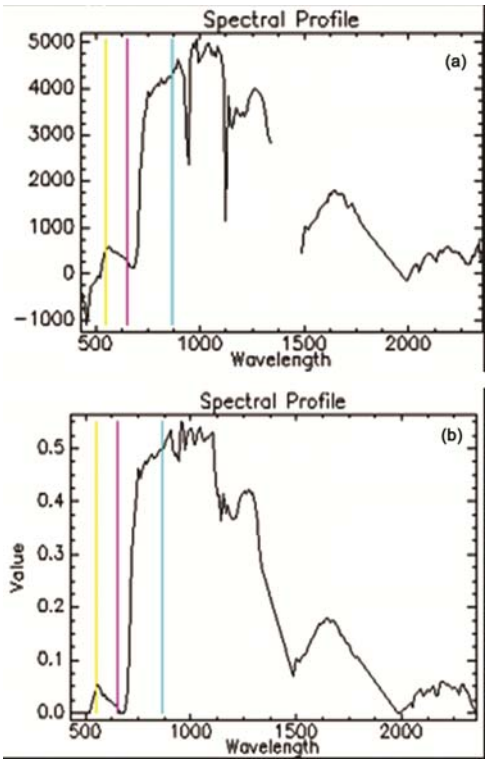

Fig. 6 — Conversion of negative value: (a) Before conversion, and (b) After conversion

amplitude of both end member spectra and spectral libraries lie between 0 to 1, it may be easy to identify the object. When one comes across for matching the end member spectra (image spectra) with the spectral libraries, it is easy to match the spectra. Figure 6(a), inferred that the negative DN occurs when the reflectance tends to decrease. After applying the

formula, the negative values are removed as shown in Figure 6(b).

(b1 le 0)*0+ (b1 ge 10000)*1+ (b1 gt 0 and b1 lt 10000)*float (b1)/1000 … (5)

The proposed system consist of various stages, (i) Selection of noisy signal, (ii) Discrete wavelet transform, (iii) Assignment of bilateral filter parameter, (iv) Inverse discrete wavelet transform, and (v) Evaluation of performance parameter. The input signal that is used in the study is the spectral profile of species of mangrove. These spectra can be derived from Analytic Spectral Devices (ASD) with the wavelength ranges from 350-2500 nm. Due to complex environment, spectral response is affected in a particular wavelength region, such as visible region of the electromagnetic spectrum. Reflectance is affected at wavelengths 350-455 nm, 1100-1450 nm, and at wavelength 2000-2500 nm by noise. In order to smoothen the spectral profile of mangrove species, the discrete wavelet transform is applied to the noisy signal to obtain the approximation and detail coefficient. Before application of bilateral filtering to low level and high level coefficient, assigning standard deviation is crucial factor to reach the desired softening of spectral profile. After that bilateral filter is applied to high and low level transformed signal, followed by reconstruction of signal.

The proposed study can be correlated with Prasad *et al*.[41], in which Moving average method and Savitzky-golay were used for noise reduction of mangrove species namely *Avicennia marina.* The same technique was executed for mangrove spectral library, but the outcome of such method is not efficient. The hybrid adaptive bilateral filtering has smoothened the signal and the noise can be eliminated as shown in Figure 7. Among the denoising techniques, HABF yield good results with PSNR and MSE value of 34.9062 and 0.0060, respectively. The

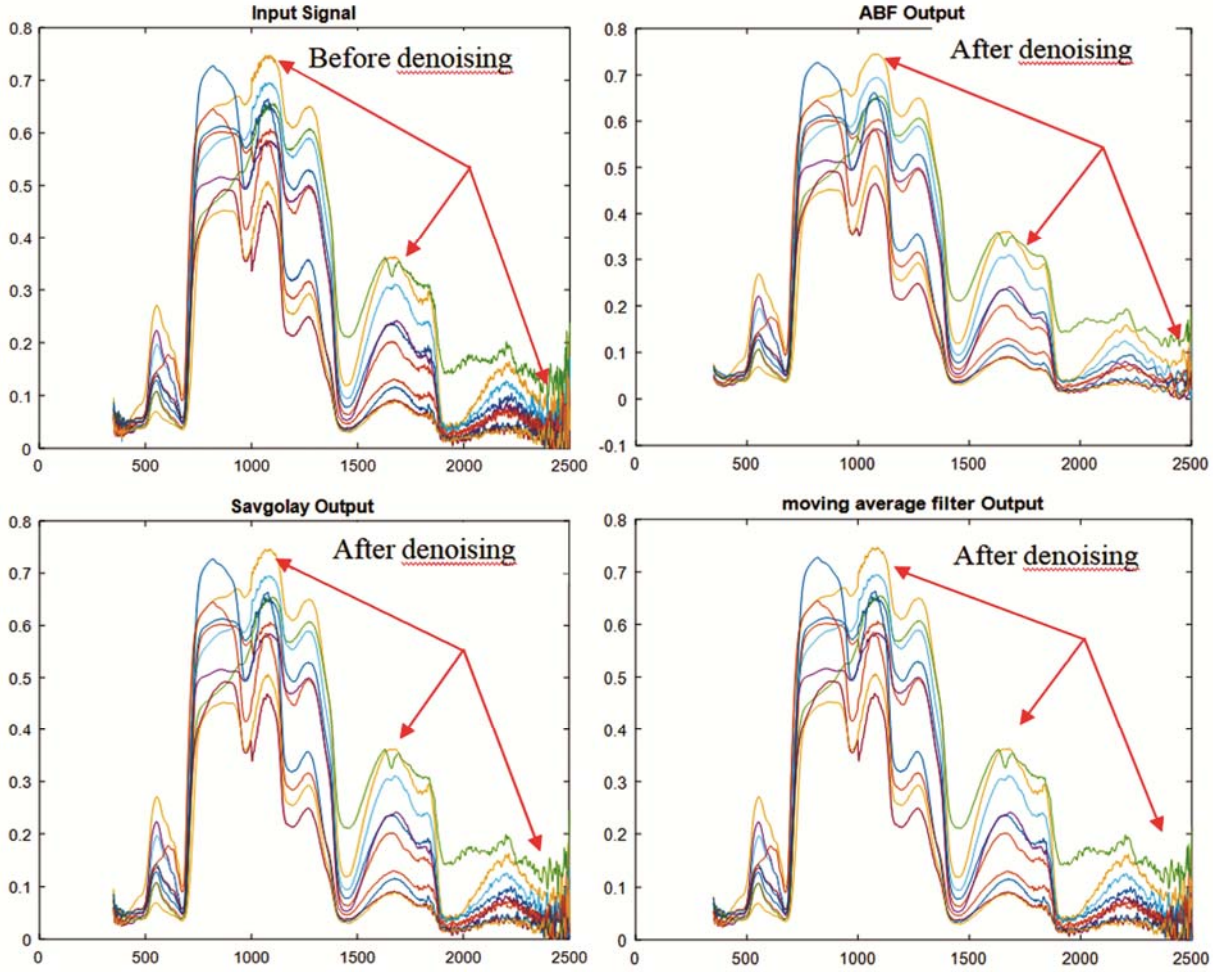

Fig.7 — Denoised signal from HABF, Savitzky-Golay, and Moving average method

Table 3 — Statics of evaluation result for four method

Denoising techniques	PSNR	MSE
HABF, This study	34.9062	0.0060
Savitzky-Golay filter	32.9029	0.0051
Moving average	31.9042	0.0050

values of PSNR and MSE for HABMF were 33.8934 and 0.0062, respectively as shown in Table 3.

Conclusion

This study attempted all necessary preprocessing steps on hyperion data and are sequentially explained. The FLAASH module provided better atmospherically corrected reflectance images and it was found that at certain times, the FLAASH model provided the negative DN pixels, which can be rectified by using the standard formula. After preprocessing procedures, the images can be used for data dimensionality and further science on image processing. This study also attempted to propose the denoising techniques for noise reduction of spectral profile of mangrove species. The field spectro-radiometer was used for generation of spectra for mangrove species, which are affected due environmental complex conditions such as moisture present in atmosphere as well as in leaf causes noise at particular wavelength. In order to obtain efficient hyperspectral image classification and interpretation, appropriate end-members are highly required. With this study, noise at wavelengths from 350-450 nm, 100-1200 nm, and 2000-2500 nm can eliminated from electromagnetic spectrum. The obtained PSNR and MSE values of hybrid adaptive bilateral filters are 34.9062 and 0.0060, respectively. Similarly for commonly used filter such as Savitzky-Golay and Moving average method, the obtained PSNR and MSE values are 32.9.9029, 0.0051, 31.9042 and 0.0050, respectively.

Acknowledgements

Authors like to express sincere thanks to USGS for providing free of cost Hyperion data, (www.earthexplorer.usgs.gov) and also extended sincere thanks to Geological survey of India-Hyperspectral division Bangalore for collection of spectra of mangrove species using field Spectro-radiometer.

Conflicts of Interest

The authors declare no conflict of interest.

Author Contributions

AS contributed towards the method and implementation of the research work and write up and SS visualized the method and research evaluation and contributed for write-up.

References

1 Goetz A F H, Kindel B C, Ferri M & Qu Z, HATCH: Results from simulated radiances, AVIRIS and Hyperion, *IEEE Trans Geosci Rem Sens*, 41 (2003) 1215–1222.

2 Miglani A, Ray S S, Pandey R & Parihar J S, Evaluation of EO-1 Hyperion Data for Agricultural Applications, *J Indian Soc Remote Sens*, 36 (2008) 255–266.

3 Hong S Y, Sudduth K A, Kitchen N R, Drummond S T, Palm H L, *et al.*, Estimating within field variations in soil properties from airborne, *Hyperspectral images, ISPRS J Photogramm Remote Sens*, 36 (2002) 255–266.

4 Abou EI-Magd I, EI-Kafrawy S & Farag I, Detecting Oil spill contamination using Airborne hyperspectral data in the River Nile, Egypt, *Open J Mar Sci*, 4 (2014) 140-150.

5 Green R O, Pavri B E & Chrien T G, On orbit radiometric and spectral calibration characteristics of EO-1 Hyperion derived with an under flight of AVIRIS and in situ Measurements at Salar de Arizaro, Argentina, *Rem Sens Environ*, 41 (2003) 1194–1203.

6 Pearlman J S, Barry P S, Segal C, Shepanski J, Beiso D, *et al.*, Hyperion, a space borne imaging spectrometer, *IEEE Trans Geosci Remote Sens*, 41 (6) (2003) 1160-117.

7 Fung T, Ma H FY & Siu W L, Band Selection Using Hyperspectral Data of Subtropical Tree Species, *Geocarto Int*, 18 (4) (2003) 3-11.

8 Ostrikov V N & Plakhothikov O V, Correlation between Hyperspectral imagery preprocessing and the quality of the thematic analysis, Izvestiya, *Izv Atmos Ocean Phys*, (9) (2014) 887-891.

9 Mitran T, Ravisankar T, Fyzee M A, Sures J R & Sujatha G, Retrieval of soil physicochemical properties towards assessing salt-affected soils using Hyperspectral Data, *Geocarto Int*, 30 (6) (2015) 701-721.

10 Vidal M & Amigo J M, Pre-processing of hyperspectral images, *Chemometr Intell Lab Syst*, 117 (2012) 138–148.

11 Meroni M, Colombo R & Panigada C, Inversion of a radiative transfer model with hyperspectral observations for LAI mapping in poplar plantations, *Rem Sens Environ*, 92 (2004) 195–206.

12 Apan A, Held A, Phinn S & Markely J, Detecting sugarcane orange rust disease using EO-1 Hyperion hyperspectral imagery, *Int J Rem Sens*, 25 (2004) 489–498.

13 Shih T Y, On the atmospheric correction for a Hyperion scene, (2004). url: http:www.arc2004.gistda.or.th/data/paper_day/B-2.pdf

14 Goetz A F H, Kindel B C, Ferri M & Qu Z, HATCH: Results from simulated radiances, AVIRIS and Hyperion, *IEEE Trans Geosci Rem Sens*, 41 (2003) 1215–1222.

15 Ganesh B P, Aravindan S, Raja S & Thirunavukkarasu A, Hyperspectral satellite data (Hyperion) preprocessing—a case study on banded magnetite quartzite in Godumalai Hill, Salem, Tamil Nadu, India, *Arab J Geosci*, 6 (2012) 3249–3256.

16 Chakravortty S & Shah E, Application of non-linear spectral unmixing on hyperspectral data for species level classification of mangroves,*ICCSP*, (2013) 1123-127

17 Pervez W, Khan S A & Valiuddin, The International Archives of the Photogrammetry, Remote Sensing and Spatial Information Sciences, *Vol XL-3/W2, 2015 PIA15+ HRIGI15 – Joint ISPRS conference*, (2015) pp. 25–27.

18 Thenkabail P S, Enclona E A, Ashton M S & Van Der M B, Accuracy assessments of hyperspectral waveband performance for vegetation analysis applications, *Rem Sens Environ*, 91 (3-4) (2004 a) 354–376.

19 Haboudane D, Miller J R, Pattey E, Zarco-Tejada P J & Strachan I B, Hyperspectral vegetation indices and novel algorithms for predicting green LAI of crop canopies: Modeling and validation in the context of precision agriculture, *Rem Sens Environ*, 90 (2004) 337–352.

20 Miglani A, Ray S S, Pandey R & Parihar J S, Evaluation of EO-1 Hyperion Data for Agricultural Applications, *J Indian Soc Remote Sens*, 36 (2008) 255–266.

21 Vignesh Kumar M & Kiran Y, Comparison of efficient techniques of hyper-spectral image preprocessing for mineralogy and vegetation studies, *Indian J Geo-Mar Sci*, 46 (2017) 1008-102.

22 Datt B, McVicar T R, Van Niel T G & Jupp D L B, Preprocessing EO-1 Hyperion hyperspectral data to support the application, IEEE Trans Geosci Remote Sens, 41 (6) (2003) 1246-1259.

23 Zheffler D & Karrasch P, Destriping of hyperspectral image data: an evaluation of different algorithms using EO-1 Hyperion data, *J Appl Remote Sens*, 8 (1) (2014).

24 Ganesh B P, Aravindan S, Raja S & Thirunavukkarasu A, Hyperspectral satellite data (Hyperion) preprocessing - a case study on banded magnetite quartzite in Godumalai Hill, Salem, Tamil Nadu, India, *Arab J Geosci*, 6 (2012) 3249–3256.

25 Ostrikov V N & Plakhothikov O V, Correlation between Hyperspectral imagery preprocessing and the quality of the thematic analysis, Izvestiya, *Izv Atmos Ocean Phy*, 9 (2014) 887-891.

26 Kale K V, Solankar M M, Nalwade D B, Dhumal R K & Gite H R, A research review on Hyperspectral data processing and Analysis algorithm, *Proc Nat Acad Sci India, Sect A*, 87 (2017) 541-555.

27 Bernstein L S, Golden S M A, Jin X, Gregor B & Sundberg R L, Quick atmospheric correction (QUAC) code for VNIR-SWIR spectral imagery: algorithm details, *4th Workshop on Hyperspectral Image and Signal Processing*, 51 (11) (2012) 111719-111729.

28 Lin J & Qu L S, Feature extraction based on morlet wavelet and its application for mechanical fault diagnosis, *J Sound Vib*, 234 (1) (2000) 132-148.

29 Selvam V, Ravichandran K K, Gnanappazham L & Navamuniyammal M, Assessment of community-based restoration of Pichavaram mangrove wetland using remote sensing data, *Curr Sci*, 85 (2003) 794–798.

30 Ramasubramanian R, Gnanappazham L, Ravishankar T & Navamuniyammal M, Mangroves of Godavari – analysis through remote sensing approach, *Wetlands Ecol Manage*, 14 (2006) 29–37.

31 Prasad K A, Gnanappazham L, Selvam V, Ramasubramanian R & Kar C S, Developing a spectral library of mangrove species of Indian east coast using field spectroscopy, *Geocarto Int*, 30 (5) (2015) 580–599.

32 Zhang H, Hyperspectral image denoising with cubic total variation model, *Remote Sens Spat Inf Sci*, 7 (2012) 95–98.

33 Yang H, Zhang D Y, Huang L S & Zhao J L, Wavelet-based threshold denoising for imaging hyperspectral data, *Int J Agric & Biol Eng*, 7 (3) (2014) 36-42.

34 Wang J H, Zhao C J & Huang W J, Basis and Application of Quantitative Remote Sensing in Agriculture, *Beijing: Science Press*, (2008) 141-184.

35 Wang Yingv & Mo Jinyuan, A New De-Noising Technique for Spectra Based on Mexican Hat Wavelet, *Spectrosc Spect Anal*, 25 (1) (2005) 124-127.

36 Zhou D, Wang Q, Tian Q, Lin Q & Fu W, *et al*., Wavelet Analysis and Its Application in Denoising the Spectrum of Hyperspectral Image, *Spectrosc Spect Anal*, 29 (7), (2009) 1941-1945.

37 Baoxin H, Qingmou L & Smith A, Noise reduction of hyperspectral data using singular spectral analysis, *Int J Remote Sens*, 30 (9) (2009) 1954-1957.

38 Longcun J, Wanggen W, Yongliang W, Bin C, Xiaoqing Y, *et al*., A General Framework for High-Dimensional Data Reduction Using Unsupervised Bayesian Model, *Commun*, 98 (2) (2010) 96-101.

39 Deivalakshmi S, Sarath S & Palanisamy P, Detection and removal of Salt and Pepper noise in images by improved median filter, *Recent Adv Intell Comput Syst*, (2011) 363-368.

40 Andria G, Attivissimo F, Cavone G, Giaquinto N & Lanzolla A M L, Linear filtering of 2-D wavelet coefficients for denoising ultrasound medical images, *Meas*, 45(7) (2012) 1792-1800.

41 Tsai F & Philpot W, Derivative Analysis of Hyperspectral Data, *Remote Sens Environ*, 66, (1998) 41-51.

42 Tomasi C & Manduchi R, Bilateral filtering for gray and color images, In: *Proc of the sixth International Conference on Computer Vision*, (IEEE Cat. No.98CH36271), January, 1998, Bombay, India. DOI: 10.1109/ICCV.1998.710692

43 King R, Ruffin C, La Mastus & Shaw D, The Analysis of Hyperspectral Data Using Savitzky-Golay Filtering – Practical Issues (Part 2), In: *IEEE 1999 International Geoscience and Remote Sensing Symposium*, IGARSS'99, (Cat. No.99CH36293), June-July, 1999. DOI: 10.1109/ IGARSS.1999.773512

44 Riechert C, Zilly F, Muller M & Kauff P, Real-time disparity estimation using line-wise hybrid recursive matching and cross-bilateral median up-sampling, In: *Proceedings of the 21st International Conference on Pattern Recognition (ICPR2012)*, November 2012, Tsukuba, Japan.